Available online at www.sciencedirect.com

ScienceDirect

Ceramics International 40 (2014) 3627–3635

CERAMICS INTERNATIONAL

www.elsevier.com/locate/ceramint

The tribological properties of bioceramic coatings produced on Ti6Al4V alloy by plasma electrolytic oxidation

Salih Durdu, Metin Usta*

The Department of Materials Science and Engineering, Gebze Institute of Technology, 41400 Gebze/Turkey

Received 14 June 2013; received in revised form 29 August 2013; accepted 14 September 2013
Available online 21 September 2013

Abstract

In this study, hydroxyapatite and calcium apatite-based bio-ceramic composite coatings were produced on Ti6Al4V alloy by plasma electrolytic oxidation (PEO) in the electrolyte consisting of calcium acetate (CA) and β-calcium glycerophosphate (β-Ca-GP) for different treatment times. Coating thickness, phase structure, coating morphology of the cross section, elemental composition, adhesion strength, wear resistance and tribological property of the PEO coatings were analyzed by eddy current method, X-ray diffraction (XRD), scanning electron microscope (SEM), energy dispersive spectroscopy (EDX mapping), micro scratch tester and tribometer, respectively. The average thickness of the coatings varied from 28 to 52 μm with increasing times. The XRD results indicated that anatase (TiO_2), rutile (TiO_2), TiP_2, TCP ($Ca_3(PO_4)_2$), perovskite – $CaTiO_3$ and hydroxyapatite ($Ca_{10}(PO_4)_6(OH)_2$) phases were formed on the Ti6Al4V alloy after PEO. According to the EDS mapping results, uniform Ca and P elemental distributions were observed on the surface of PEO coatings. The adhesion strengths of the PEO coatings enhanced with increasing time. The wear resistances and tribological properties of the PEO coatings were greater than those of the uncoated Ti6Al4V alloys, and they were increased with increased time.

Keywords: Plasma electrolytic oxidation; Micro arc oxidation; Hydroxyapatite coatings; Titanium alloys; Mechanical properties

1. Introduction

Titanium and its alloys have been widely used in medical, orthopedic and dental implant materials because of their high load strength bearing capacity, high strength to weight ratio, low toxicity, chemical stability, superior mechanical properties, excellent corrosion resistance and high biocompatibility [1–3]. However, titanium and its alloys exhibit poor bioactivity [4]. In addition, they are not chemically integrated with bone tissue, although they directly connect to the bone [5,6]. Therefore, the hydroxyapatite ($Ca_{10}(PO_4)_6(OH)_2$), which exists in bone structure and consists of about 70% weight of bone, is coated on titanium implant surface. The hydroxyapatite provides chemical bonding between bone and implants owing to its biological and chemical similarity to the body hard tissues such as bone [7,8]. The hydroxyapatite which improves the bone tissue osseointegration is bioactive and biocompatible for biomedical applications [9,10]. However, the hydroxyapatite is not used in load bearing applications due to the poor mechanical properties [11]. Thus, their osteoconductive properties of hydroxyapatite are combined with superior mechanical properties of titanium and its alloys by using various coating processes such as plasma spray coating [12–14], electrochemical deposition [14], electrophoretic deposition [15,16], sol–gel technique [17,18], immersion in SBF (simulated body fluid) [19], laser ablation [20] and bio-mimetic techniques [21], etc. Among them; the hydroxyapatite coatings produced by the plasma spray method are widely used in the bio-medical sector. However, the hydroxyapatite coatings produced by the plasma spray method have some problems such as chemical in-homogeneity, structure control, maintaining phase purity, poor fracture toughness and adhesion strength [22–25].

The plasma electrolytic oxidation (PEO) produces thick, hard and strong ceramic coatings on Ti, Mg, Al, Zr and their alloys by electrochemical oxidation process [26–29]. The PEO technique is also called as micro arc oxidation (MAO), anodic spark oxidation or micro plasma oxidation. The PEO is based on the principle of anodic oxidation of light metals and alloys

*Corresponding author. Tel.: +90 262 605 2655; fax: +90 262 605 8490.
E-mail addresses: sdurdu@gyte.edu.tr (S. Durdu), ustam@gyte.edu.tr (M. Usta).

0272-8842/$ - see front matter © 2013 Elsevier Ltd and Techna Group S.r.l. All rights reserved.
http://dx.doi.org/10.1016/j.ceramint.2013.09.062

such as Ti, Al, Mg in aqueous electrolyte solutions under a condition of plasma discharge at exceeding the critical values of the polarization potential [30,31]. The major advantage of PEO process is the possibility of incorporating Ca and P ions into the titanium surface by controlling the coating parameters such as composition of the electrolyte, applied voltage, current density and treatment times [32,33]. The Ca^{2+} and PO_4^{3-} ions, which occur at high temperatures in micro discharge channels during PEO process, react with each other to form the hydroxyapatite phase in the coatings [34,35]. The existence of the hydroxyapatite on the surface increases the bioactivity potential of titanium implant. In addition, the PEO coatings which are uniformly coated on complex shaped metal surfaces are thick and porous [36]. These porous surfaces produced by the PEO method beneficially contributes to cell attachment, propagation and bone growth in biomedical implant applications. The average pore sizes of the PEO coatings that depend on coating time, voltage and electrolyte composition can vary between 1 and 20 μm as given in the literature [34].

The hydroxyapatite coatings on titanium and its alloys by plasma electrolytic oxidation are presented in the literature [22,23,33,37,38]. However, in various studies, a two- step process has been used for formation of hydroxyapatite. In the first step, titanium or its alloys were coated by PEO in an alkaline aqueous electrolyte to produce the oxide ceramic surface. This oxide surface contributes to the formation of hydroxyapatite on the metal. As the second step, the PEO coatings were placed in the bottom of autoclave and hydrothermally treated at high temperatures for long duration times [22,23,37] or immersed in the SBF (simulated body fluid) and kept under body temperature conditions (36.5 °C) up to long times (56 days) [33] or recoated to form hydroxyapatite by the sol–gel method [38]. In our previous study, the hydroxyapatite and calcium apatite-based phases such as TCP, $CaTiO_3$ were directly formed on Ti6Al4V surface coated by PEO method in a single step. The formation of hydroxyapatite and other calcium apatite-based phases were investigated and characterized by XRD, SEM, XPS and ATR FT-IR [34]. There are no reports on the mechanical and tribological properties of hydroxyapatite coatings on titanium and its alloys by one-step PEO in the literature, although there are some studies in the literature [39–42] on the wear properties of only TiO_2 based coatings on titanium and its alloys produced by the PEO method. In a different study, the wear properties of micro arc oxidized and hydrothermal treated Ti6Al4V were investigated by Vangolu et all [41]. However, the mechanical and wear properties of hydroxyapatite-based phases directly formed on the Ti6Al4V coated by one-step PEO method has not been investigated in the literature.

2. Experimental details

2.1. Materials and preparation of PEO coatings

The rectangular samples (65 mm × 25 mm × 5 mm) of Ti6Al4V alloys were used as substrates. The surface of the Ti6Al4V specimens was ground by using 400, 800 and 1200 grids SiC papers. And then, the specimens were cleaned in distilled water and acetone. The coatings were produced on Ti6Al4V specimens by using plasma electrolytic oxidation (PEO). The PEO method was carried out in the electrolyte, containing calcium acetate ($Ca(OOCCH_3)_2 \cdot xH_2O$) and β-calcium glycerophosphate (β-$C_3H_7CaO_6P$) at 0.123 A/cm^2 current density for 20, 40, 60 and 90 min. The PEO equipment (100 kW) was composed of an AC power supply, a stainless steel container as well as cooling and stirring systems. For this process, the titanium substrate was used as the anode, while the stainless steel container was used as the cathode. The temperature in the electrolyte was maintained below 30 °C during the PEO process. After the PEO, the coatings were washed with distilled water and dried out under the warm air.

2.2. Characterization of the coatings

The thickness of the PEO coatings was measured by using an eddy current method (Fischer Dualscope MP40) at 20 randomly selected locations. The phase structures of the PEO coatings and uncoated Ti6Al4V substrate were detected by X-ray diffraction method (XRD; Bruker D8 Advance) using Cu-Kα radiation between 20° and 80° angles with a step size 0.02° /min. The cross-sectional morphologies of the coatings were examined by scanning electron microscope (SEM; Philips XL30 SFEG). The elemental mappings of the coatings were analyzed by energy dispersive spectroscopy (EDX-Mapping).

The adhesion strengths of the coatings to the substrate were evaluated by the micro scratch tester (Nanovea Series). The progressive load was applied from 0.3 to 10 N along five mm on the PEO coatings. The critical loads (Lc1, Lc2 and Lc3) at which adhesive failure of the coating occurred were determined by optical microscope imaging of the scratch track after the test. Lc was used as a measure for the coating bonding strength. The friction and wear tests on the coatings were carried out on a ball-on-disk tribometer (CSM Instruments) under dry experiment conditions at room temperature (25 °C) in the ambient atmosphere. An alumina ball with the diameter of 6 mm was tightly fixed in the ball holder as the static friction partner against the PEO coatings and uncoated Ti6Al4V. The wear test was carried out at a normal load of 1 N samples reciprocated against the ball with the maximum linear speed of 5 cm/s, amplitude of 8.5 mm and the cycles of 2941.

3. Results and discussion

3.1. Phase structure of the coatings (XRD)

Fig. 1 illustrates the X-ray diffraction patterns of the PEO coatings produced at different treatment times and uncoated Ti6Al4V alloy. The anatase – TiO_2, rutile – TiO_2, TiP_2 (Titanium phosphide), $Ca_3(PO_4)_2$ (TCP-tri calcium phosphate), perovskite – $CaTiO_3$ and $Ca_{10}(PO_4)_6(OH)_2$ (Hydroxyapatite) phases were obtained on the PEO surfaces; and only the Ti peaks were detected on Ti6Al4V alloy.

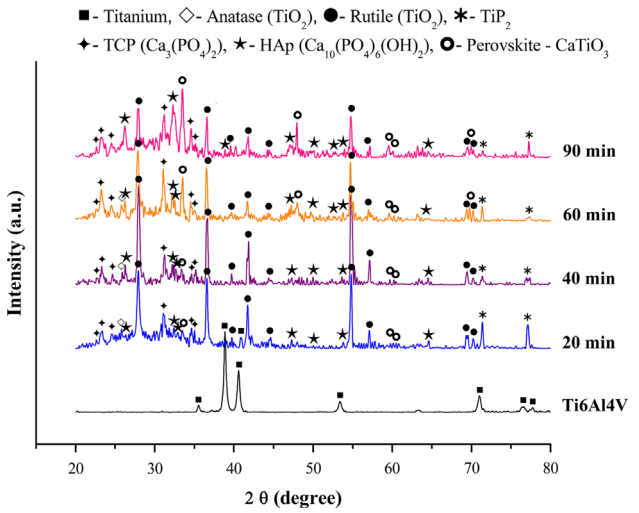

Fig. 1. The X-ray diffraction patterns of the PEO coatings produced at different duration times and uncoated Ti6Al4V alloy.

The anatase – TiO_2 as a minor phase and rutile – TiO_2 as a major phase exist in the PEO coatings produced at all treatment times. The anatase and rutile phases on the surface are formed by the reacting of Ti^{4+} and OH^- ions under high temperature and high pressure in micro discharge channels during PEO process. The anatase forms earlier than rutile due to the effect of low temperatures in micro discharge channels at initial stages of PEO process. And then, it transforms into rutile with increasing treatment times, current density or applied voltage during PEO process because the stable phase of TiO_2 is rutile at high temperatures [34,43]. The anatase–rutile transition does not take place at a definite temperature, and the transition temperatures range between 700 and 1300 K [44]. Moreover, it is claimed in the literature [45,46] that the local temperatures in micro discharge channels vary from 800–3000 K to 2000–10,000 K because of electron collision during PEO process. The amount of anatase and rutile increases up to 40 min. And then, they decrease in the coating produced from 60 to 90 min. In addition, the Ca^{2+} and PO_4^{3-} ions, which come from electrolyte consisting of CA and β-Ca-GP, react with Ti^{4+} and OH^- ions. And then, perovskite phase forms in the coating structure as shown in Fig. 1. After 40 min, the amount of perovskite increases while the amount of anatase and rutile decrease in the coating structure. It is concluded that the Ca^{2+}, Ti^{4+} and OH^- ions react to form perovskite – $CaTiO_3$ due to the existence of high temperature in micro discharge channels with increasing treatment time. The TCP, which forms in the PEO coating produced at all treatment times exists during PEO process. Up to 60 min, the amount of TCP increases in the coating structure. After 60 min, the TCP phase begins to dissolve and the amount of it decreases as seen in Fig. 1. The TCP is formed by the reactions between Ca^{2+} and PO_4^{3-} ions in micro discharge channels. Similarly, the hydroxyapatite phase presents in the coating produced at all treatment times. In addition, the amount of hydroxyapatite increases with treatment time. The formation mechanism of hydroxyapatite is similar to the one of TCP; however, unlike the formation of TCP, the Ca^{2+} and PO_4^{3-} ions that come from the electrolyte to form hydroxyapatite react with H_2O molecules. It can be concluded that crystallization of perovskite – $CaTiO_3$ and hydroxyapatite were enhanced by increasing time. In addition, the decomposition of TCP is highly effective on the forming of hydroxyapatite after 60 min. As a result, the local temperature in micro discharge channels rises with increasing duration time. This situation contributes to form crystalline perovskite – $CaTiO_3$ and hydroxyapatite during PEO process as seen from XRD results. The phase structures of uncoated Ti6Al4V alloy and the PEO coatings are given in Table 1.

Table 1
The phase structures of uncoated Ti6Al4V alloy and the PEO coatings.

Coating time ($_{min}$)	The phase structure
Substrate	Titanium
20	Titanium, Anatase, Rutile, Titanium phosphide, TCP, Perovskite – $CaTiO_3$, HAp
40	Anatase, Rutile, Titanium phosphide, TCP, Perovskite – $CaTiO_3$, HAp
60	Anatase, Rutile, Titanium phosphide, TCP, Perovskite – $CaTiO_3$, HAp
90	Rutile, Titanium phosphide, TCP, Perovskite – $CaTiO_3$, HAp

3.2. Elemental mapping of the coatings (EDX-mapping)

Fig. 2(a)–(d) shows the elemental mapping results of the PEO coatings produced at 20, 40, 60 and 90 min, respectively. The elements of Ti, O, Ca, P and Al are observed on the PEO coatings. The concentrations of the Ca and P increase with increasing duration time as seen in Fig. 2(a)–(d). The elements of Ca and P in the electrolyte consisting of CA and β-Ca-GP ionize due to the existence of electric field during PEO process. Afterwards, they react with each other in micro discharge channels. The elements of Ca and P required to form hydroxyapatite enter the coating structure with increasing time. And then, they react with each other and oxygen. The Ca and P exist as amorphous structure on the outer surface of coating owing to the rapid cooling rate of melted compounds during PEO process [34,47]. The elements of Ca and P are uniformly distributed on the coating surfaces as seen in Fig. 2 (a)–(d). The elements of Ca and P cause the formation of the hydroxyapatite and calcium apatite-based phases as major phases with increasing duration time because they exist as dominant elements in the coating. As a result of these mapping images, it can be concluded that the hydroxyapatite and calcium apatite-based phases are homogenously distributed on the PEO coating surfaces.

3.3. Cross sectional morphologies of the coatings (SEM)

Fig. 3(a)–(d) shows the cross-sectional morphologies of the PEO coatings produced at 20, 40, 60 and 90 min, respectively. The thickness of the PEO coatings enhances with increasing duration time as seen in Fig. 3. Furthermore, the size of the pores in the coating structure increases with duration time. The

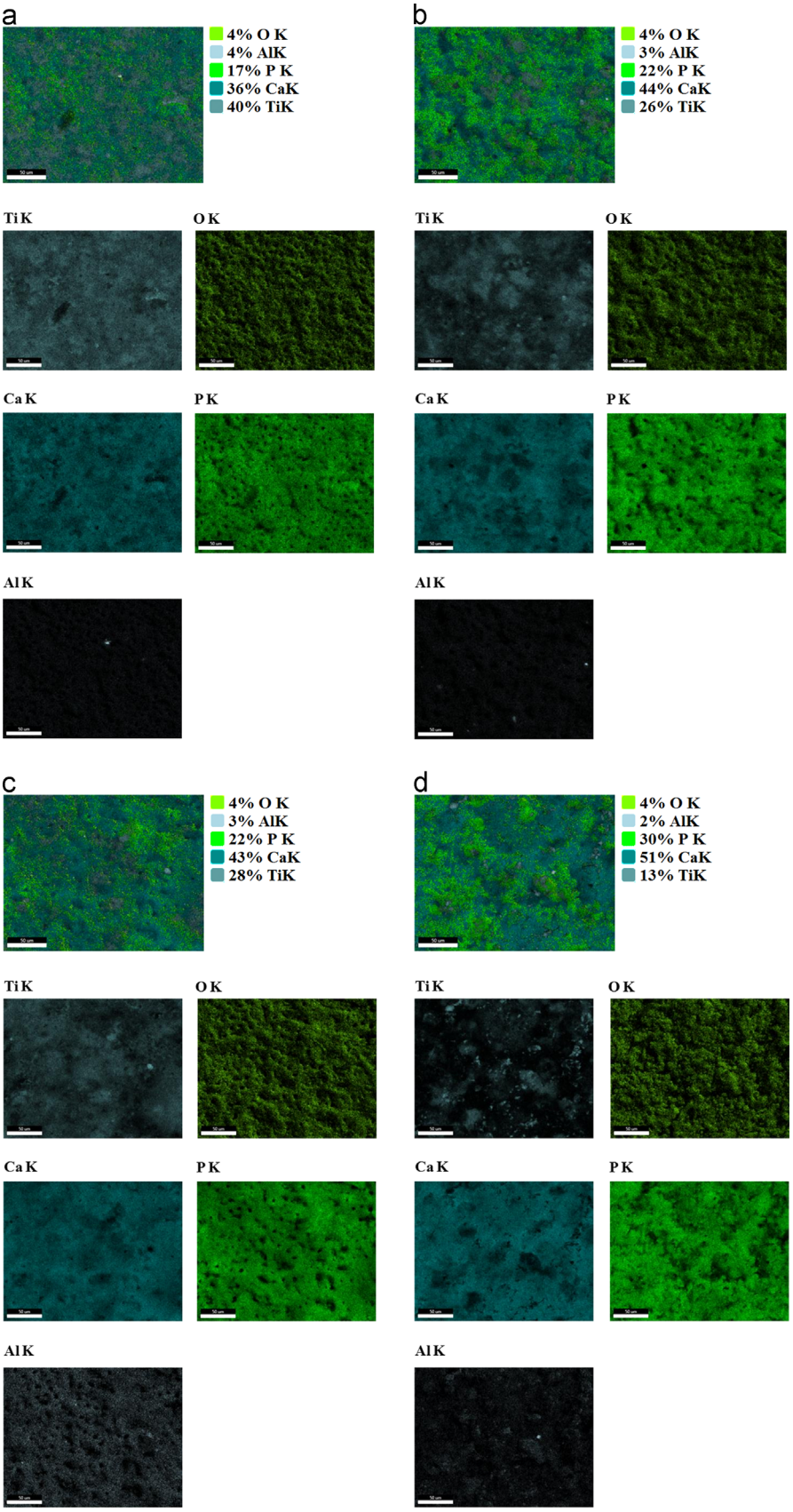

Fig. 2. The elemental mapping results of the PEO coatings produced at different duration times: (a) 20 min, (b) 40 min, (c) 60 min and (d) 90 min.

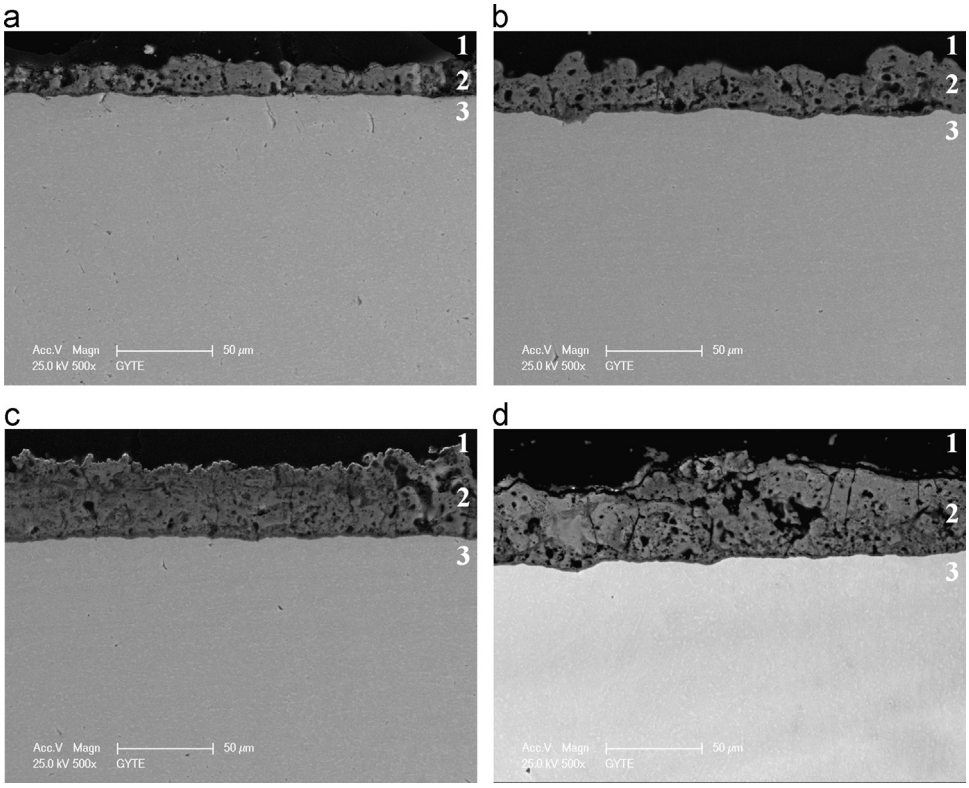

Fig. 3. The cross sectional SEM morphologies of the PEO coatings produced at different duration times: (a) 20 min, (b) 40 min, (c) 60 min and (d) 90 min: (1) epoxy resin region, (2) PEO coating region and (3) substrate region.

PEO coatings are very porous and rough due to the existence of micro discharges during PEO process. The outer layer of the PEO coatings is amorphous owing to the rapid cooling rate of electrolyte. In addition, the interior layer of the PEO coatings is crystalline and dense due to the effects of high temperature and high pressure. Therefore, the inner layer of the coatings is denser and harder than the outer layer of the coatings. The thickness of dense layer which is close to substrate increases with duration time as seen in Fig. 3. However, the coating produced at 60 min is denser than the one produced at 90 min due to the increased the sizes of pores. Table 2 shows the average pore sizes of the PEO coatings produced at different coating times. The coatings that have a dense and hard layers exhibit greater mechanical and tribological properties than one with the porous layers [30]. Thus, the thicker and the denser layer show greater coating quality in terms of excellent the mechanical and tribological properties.

Table 2
The average pore sizes of the PEO coatings via the coating times.

Coating time ($_{min}$)	The average pore size (μm)
20	6
40	7
60	8
90	15

3.4. Adhesion strength of the coatings

The adhesion strength of the PEO coatings produced on Ti6Al4V at different treatment times was measured by the micro scratch tester. The micro scratch test results obtained at 200 μm radius Rockwell C diamond tip for PEO coatings were given in Table 3. The critical load, Lc1, which occurs as the first failure, corresponds to initial cracking. Lc2, which occurs as the second failure, corresponds to extensive cracking. Lc3, which occurs as the final failure, corresponds to delamination of the coating from the titanium surface. The critical load values such as Lc1–Lc3 at which failures of the coatings occurred were determined by optical microscopy examination of the scratch track after the test. The Lc values measured after the scratch test is a characteristic value for each coating. The Lc values depend on various parameters such as thickness, hardness, and phase structure. Load carrying capacity of the coating increases by varying these parameters as reported in the literature [48]. Therefore, the higher critical load is, the greater adhesion and bonding strength of the coatings are provided for each coating.

Fig. 4(a)–(d) illustrates the load–sliding distance curve and optical micro graph imaging of the PEO coatings produced at 20, 40, 60 and 90 min, respectively. After the scratch test, an adhesive failure at the edge of scratch track and cohesive failure in the inner layer of scratch track occur as seen in Fig. 4 (a)–(c). It is reported in the literature [49] that increasing cohesion strength prevents the coating from detachment of particles. As a result of increasing applying load and critical load, the coating is removed from the substrate. In addition, the

Table 3
Experimental scratch test results obtained at 200 μm radius tip for PEO coatings produced at different coating times.

Coating time ($_{min}$)	Average thickness (μm)	Lc1			Lc2			Lc3		
		Normal load (N)	Frictional force (N)	Distance (mm)	Normal load (N)	Frictional force (N)	Distance (mm)	Normal load (N)	Frictional force (N)	Distance (mm)
20	33.0 ± 0.7	4.434	2.815	2.274	4.851	2.863	2.495	5.214	3.801	2.581
40	42.7 ± 1.7	4.743	2.822	2.146	4.952	2.781	2.322	5.382	3.308	2.432
60	47.0 ± 1.9	5.282	3.671	2.514	6.230	3.192	2.907	6.654	4.890	3.116
90	52.2 ± 3.4	–	–	–	–	–	–	–	–	–

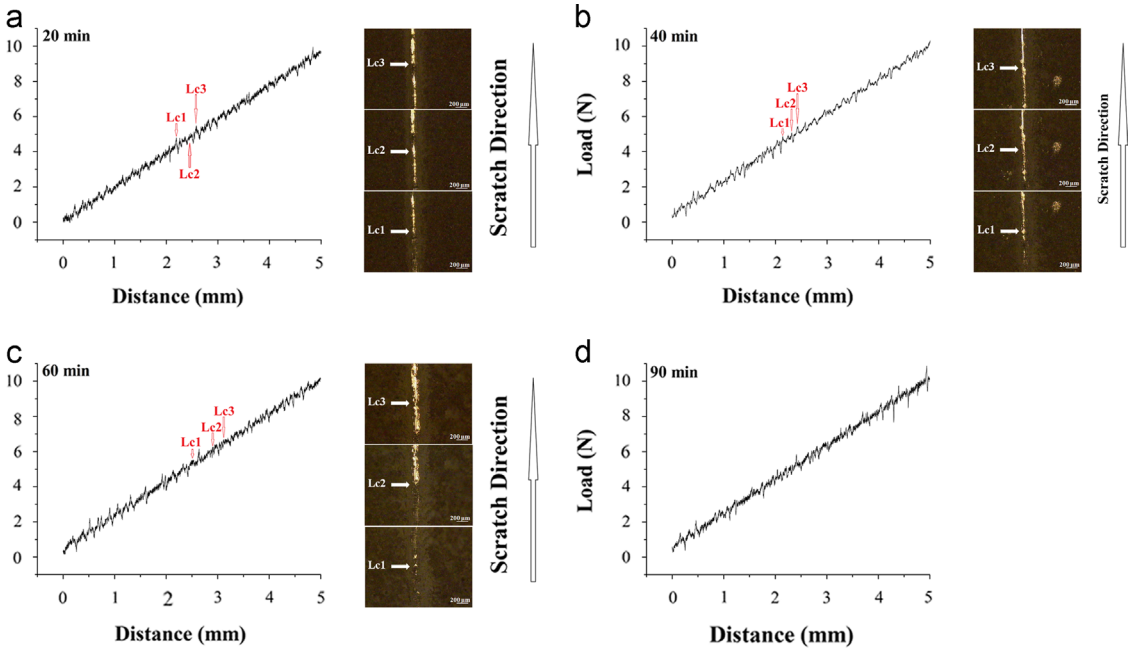

Fig. 4. The load–distance curves and optical micro graph imaging of the PEO coatings produced at different duration times: (a) 20 min, (b) 40 min, (c) 60 min and (d) 90 min.

Table 4
Wear test results obtained under dry conditions for uncoated Ti6Al4V and PEO coatings.

Coating time ($_{min}$)	Sample wear rate (mm^3/N m)	Sample worn track section (μm^2)
Substrate	18.8×10^{-4}	5516.0
20	3.74×10^{-4}	1099.9
40	3.17×10^{-4}	933.5
60	0.48×10^{-4}	141.5
90	1.64×10^{-4}	484.3

thickness of the coatings increased with duration times due to fact that a larger volume metal enters into micro discharge channels during PEO process. This is one of the effective factors to increase the adhesion strength of the PEO coatings with increasing of duration time as seen in Table 1. There is no failure for the coating produced at 90 min, although the coating produced at 90 min is more porous and looser than the one produced at 60 min. This could be explained by high coating thickness and the existence of the high amount of perovskite – $CaTiO_3$ in the structure because the $CaTiO_3$ increased adhesion strength between the titanium substrate and hydroxyapatite based coating structure [50]. In addition, the hardness of dense perovskite – $CaTiO_3$ is 8.0 ± 0.2 GPa [51]. It can be concluded that the dominant parameters for adhesion strength of the coatings are phase structure, hardness and thickness of the coating.

3.5. Wear resistance of the coatings

The wear rates of the PEO coatings and uncoated Ti6Al4V alloy are summarized in Table 4. The wear rates of PEO coatings were between 0.48×10^{-4} and 3.74×10^{-4} mm^3/N m while the wear rate of Ti6Al4V was determined as 18.8×10^{-4} mm^3/N m. The wear mechanism of Ti6Al4V alloy refers to adhesive type as seen in Fig. 5(a). This is because Al_2O_3 ball is harder than the one of Ti6Al4V alloy [52]. There are many plastic deformations on the worn track of the Ti6Al4V alloy. Therefore, the wear mechanism of Ti6Al4V combined with a little adhesive wear is dominantly abrasive wear.

The wear resistance of the PEO coatings was significantly improved. The wear rates of the PEO coatings produced at 20, 40, 60 and 90 min were measured as 3.74×10^{-4}, 3.07×10^{-4},

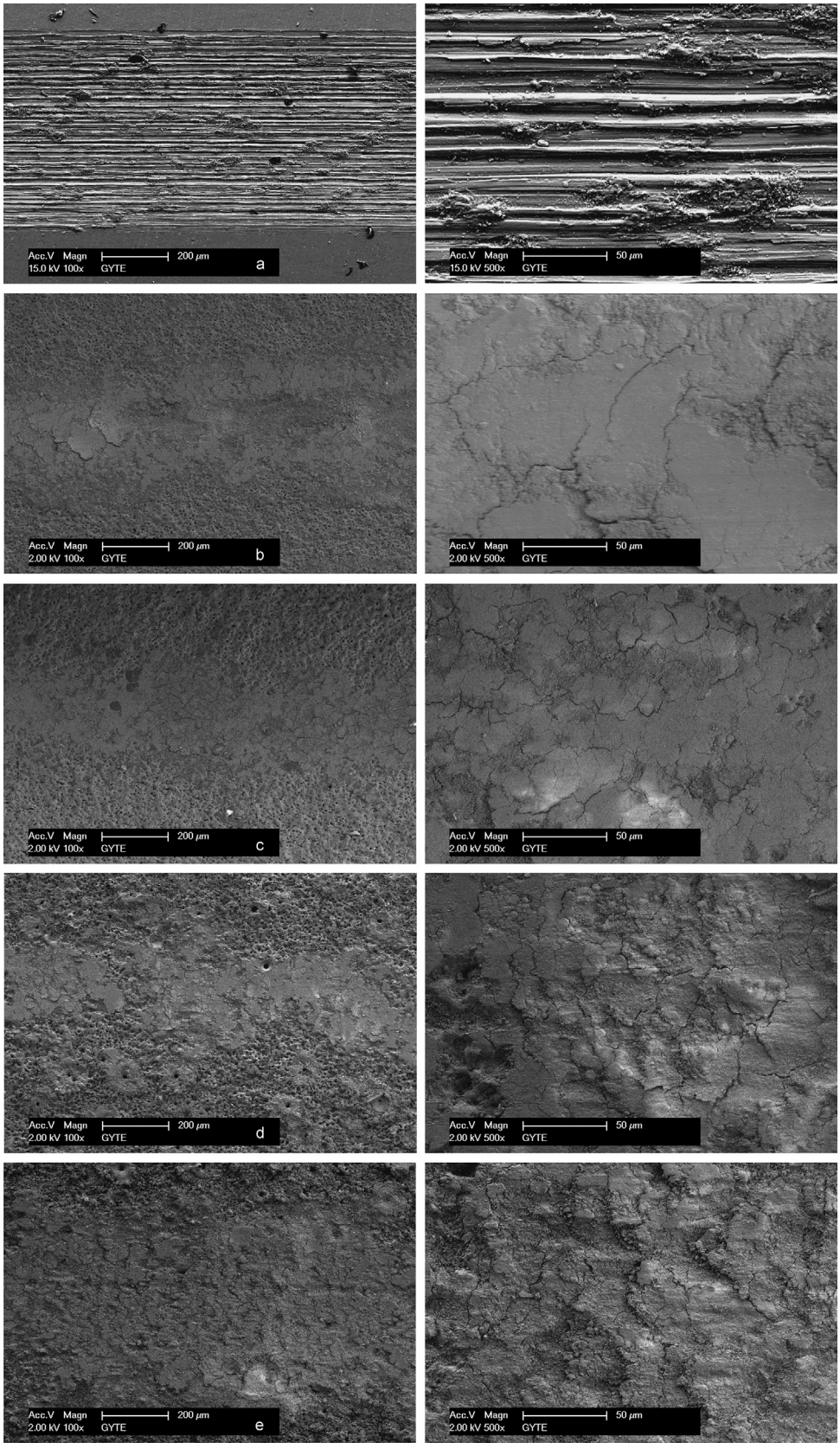

Fig. 5. The wear tracks of untreated Ti6Al4V alloy and the PEO coatings: (a) Ti6Al4V, (b) 20 min, (c) 40 min, (d) 60 min and (e) 90 min.

0.48×10^{-4} and 1.64×10^{-4} mm^3/N m, respectively. Generally, the wear resistance of the PEO coatings increases with coating time as indicated in the wear results. However, the wear rate of coating produced at 90 min is higher than the one produced at 60 min because the coating produced at 60 min is denser than the one produced at 90 min as seen in Fig. 3. It can be concluded that the wear resistance of the coatings depends on the morphology and the phase structure of the coatings.

Fig. 5(a)–(e) shows the wear track SEM images of the uncoated Ti6Al4V alloy and the PEO coatings produced at 20, 40, 60 and 90 min, respectively. The wear track of Ti6Al4V alloy is wider and deeper than the ones of PEO coatings as seen in Fig. 5. The coatings produced by the PEO method are very rough and have much porosity due to the presence of micro discharge channels during the process. The outer layer of the PEO coatings is looser and softer than the inner layer of the PEO coatings. Therefore, the fine crumbs or particles on the outer layer of the PEO occur during the wear test. The fine crumbs or particles were removed from the outer surface during the wear test. It is assumed that these fine crumbs or particles act as a lubricant between dense coating layer and Al_2O_3 ball through wear test, leading to less wear rates of the coatings. After the wear test, the micro cracks were observed on the wear tracks as seen in Fig. 5(b)–(e). The long micro cracks occur on the surface after the wear test because the PEO coatings produced at high duration times are very porous and rough. The average surface roughness of the PEO coatings produced at 20, 40, 60 and 90 min measured as 2.26, 2.21, 3.00 and 4.50 μm. In addition, after the wear test, the compact coating structure appears under the outer layer because the exterior layer of the PEO coatings with low hardness is very porous, rough and loose. As a result, it is concluded that wear mechanism of the PEO coatings is an abrasive type due to the presence of the fine crumb particles during the wear test.

4. Conclusions

The hydroxyapatite and calcium apatite-based phases such as TCP and perovskite – $CaTiO_3$ were coated on Ti6Al4V alloy at different duration times in the electrolyte consisting of CA and β-Ca-GP by PEO method. The mechanical properties such as adhesion strength and wear properties of hydroxyapatite-based PEO coatings were investigated in detail. The following results were obtained as below:

1. The PEO coatings contained TiO_2, TiP_2, TCP ($Ca_3(PO_4)_2$), perovskite – $CaTiO_3$ and hydroxyapatite ($Ca_{10}(PO_4)_6(OH)_2$) phases. The amount and the intensity of hydroxyapatite and calcium apatite-based phases increased with coating time. Hydroxyapatite and perovskite – $CaTiO_3$ were observed as major phases at the coating produced at 90 min.
2. According to the EDX mapping results, Ca and P elements were uniformly distributed on the PEO coatings. In addition, the amounts of Ca and P increased with coating time.
3. The PEO coatings adhered much firmly to the Ti6Al4V metal. The adhesion strength of the PEO coatings increased with coating time. There was no failure and delamination at the coating produced at 90 min due to the high thickness and the presence of perovskite – $CaTiO_3$ phase. This indicates that the greater adhesion strength of the PEO coating is produced at 90 min.
4. The PEO coatings significantly improved the wear resistance of Ti6Al4V alloy. The wear properties of the PEO coatings increased with increasing duration time, although the wear resistance of the coating produced at 90 min is lower than the one produced at 60 min. This could be due to the fact that the coating produced at 90 min is much porous and looser than the one produced at 60 min.

Acknowledgments

The authors would like to thank Mr. S. Levent Aktug for running X-ray diffraction (XRD) and Mr. A. Nazim for running scanning electron microscope (SEM) and energy dispersive spectroscopy (EDX-Mapping) at Gebze Institute of Technology.

References

[1] W.H. Song, H.S. Ryu, S.H. Hong, Antibacterial properties of Ag (or Pt)-containing calcium phosphate coating formed by micro-arc oxidation, Journal of Biomedical Materials Research Part A 88A (1) (2009) 246–254.
[2] A. Alsaran, G. Purcek, I. Hacisalihoglu, Y. Vangolu, O. Bayrak, I. Karaman, A. Celik, Hydroxyapatite production on ultrafine-grained pure titanium by micro-arc oxidation and hydrothermal treatment, Surface & Coatings Technology 205 (2011) S537–S542.
[3] K.C. Kung, T.M. Lee, T.S. Lui, Bioactivity and corrosion properties of novel coatings containing strontium by micro-arc oxidation, Journal of Alloys and Compounds 508 (2) (2010) 384–390.
[4] D.Q. Wei, Y. Zhou, C.H. Yang, Characteristic, cell response and apatite-induction ability of microarc oxidized TiO_2-based coating containing P on Ti6Al4V before and after chemical-treatment and dehydration, Ceramics International 35 (7) (2009) 2545–2554.
[5] F. Samanipour, M.R. Bayati, F. Golestani-Fard, H.R. Zargar, T. Troczynski, A.R. Mirhabibi, An innovative technique to simply fabricate ZrO_2–HA–TiO_2 nanostructured layers, Colloids and Surfaces B-Biointerfaces 86 (1) (2011) 14–20.
[6] M.A. Faghihi-Sani, A. Arbabi, A. Mehdinezhad-Roshana, Crystallization of hydroxyapatite during hydrothermal treatment on amorphous calcium phosphate layer coated by PEO technique, Ceramics International 39 (2) (2013) 1793–1798.
[7] L.P. Ward, K.N. Strafford, T.P. Wilks, C. Subramanian, The role of refractory element based coatings on the tribological and biological behaviour of orthopaedic implants, Journal of Materials Processing Technology 56 (1–4) (1996) 364–374.
[8] M. Hekmatfar, S. Moshayedi, S.A. Ghaffari, H.R. Rezaei, F. Golestani-Fard, Fabrication of HAp–8YSZ composite layer on Ti/TiO2 nanoporous substrate by EPD/MAO method, Materials Letters 65 (23–24) (2011) 3421–3423.
[9] A. Nanci, J.D. Wuest, L. Peru, P. Brunet, V. Sharma, S. Zalzal, M. D. McKee, Chemical modification of titanium surfaces for covalent attachment of biological molecules, Journal of Biomedical Materials Research 40 (2) (1998) 324–335.
[10] D.Y. Lin, X.X. Wang, A novel method to synthesize hydroxyapatite coating with hierarchical structure, Colloids and Surfaces B-Biointerfaces 82 (2) (2011) 637–640.
[11] D.Q. Wei, Y. Zhou, Y.M. Wang, D.C. Jia, Characteristic of microarc oxidized coatings on titanium alloy formed in electrolytes containing

chelate complex and nano-HA, Applied Surface Science 253 (11) (2007) 5045–5050.
[12] J. Weng, Q. Liu, J.G.C. Wolke, X.D. Zhang, K. deGroot, Formation and characteristics of the apatite layer on plasma-sprayed hydroxyapatite coatings in simulated body fluid, Biomaterials 18 (15) (1997) 1027–1035.
[13] V.J.P. Lim, K.A. Khor, L. Fu, P. Cheang, Hydroxyapatite–zirconia composite coatings via the plasma spraying process, Journal of Materials Processing Technology 90 (1999) 491–496.
[14] B.G. Boe, S.M. Rohrl, T. Heier, F. Snorrason, L. Nordsletten, A prospective randomized study comparing electrochemically deposited hydroxyapatite and plasma-sprayed hydroxyapatite on titanium stems, Acta Orthopaedica 82 (1) (2011) 13–19.
[15] L. Mohan, D. Durgalakshmi, M. Geetha, T. Narayanan, R. Asokamani, Electrophoretic deposition of nanocomposite (HAp + TiO_2) on titanium alloy for biomedical applications, Ceramics International 38 (4) (2012) 3435–3443.
[16] J. Ma, C. Wang, K.W. Peng, Electrophoretic deposition of porous hydroxyapatite scaffold, Biomaterials 24 (20) (2003) 3505–3510.
[17] C.S. Chai, B. Ben-Nissan, Bioactive nanocrystalline sol–gel hydroxyapatite coatings, Journal of Materials Science-Materials in Medicine 10 (8) (1999) 465–469.
[18] M.-F. Hsieh, L.-H. Perng, T.-S. Chin, Hydroxyapatite coating on Ti6Al4V alloy using a sol–gel derived precursor, Materials Chemistry and Physics 74 (3) (2002) 245–250.
[19] L.H. Long, L.D. Chen, S.Q. Bai, J. Chang, K.L. Lin, Preparation of dense beta-$CaSiO_3$ ceramic with high mechanical strength and HAp formation ability in simulated body fluid, Journal of the European Ceramic Society 26 (9) (2006) 1701–1706.
[20] L. Cleries, J.M. Fernandez-Pradas, J.L. Morenza, Behavior in simulated body fluid of calcium phosphate coatings obtained by laser ablation, Biomaterials 21 (18) (2000) 1861–1865.
[21] P. Habibovic, F. Barrere, C.A. van Blitterswijk, K. de Groot, P. Layrolle, Biomimetic hydroxyapatite coating on metal implants, Journal of the American Ceramic Society 85 (3) (2002) 517–522.
[22] F. Liu, F.P. Wang, T. Shimizu, K. Igarashi, L.C. Zhao, Formation of hydroxyapatite on Ti–6Al–4V alloy by microarc oxidation and hydrothermal treatment, Surface & Coatings Technology 199 (2-3) (2005) 220–224.
[23] F. Liu, F.P. Wang, T. Shimizu, K. Igarashi, L.C. Zhao, Hydroxyapatite formation on oxide films containing Ca and P by hydrothermal treatment, Ceramics International 32 (5) (2006) 527–531.
[24] L.L. Yan, Y. Leng, L.T. Weng, Characterization of chemical inhomogeneity in plasma-sprayed hydroxyapatite coatings, Biomaterials 24 (15) (2003) 2585–2592.
[25] F.J. GarciaSanz, M.B. Mayor, J.L. Arias, J. Pou, B. Leon, M. PerezAmor, Hydroxyapatite coatings: a comparative study between plasma-spray and pulsed laser deposition techniques, Journal of Materials Science-Materials in Medicine 8 (12) (1997) 861–865.
[26] S. Stojadinovic, R. Vasilic, M. Petkovic, B. Kasalica, I. Belca, A. Zekic, L. J. Zekovic, Characterization of the plasma electrolytic oxidation of titanium in sodium metasilicate, Applied Surface Science 265 (2013) 226–233.
[27] S. Durdu, S. Bayramoglu, A. Demirtas, M. Usta, A.H. Ucisik, Characterization of AZ31 Mg Alloy coated by plasma electrolytic oxidation, Vacuum 88 (2013) 130–133.
[28] S. Stojadinovic, R. Vasilic, I. Belca, M. Petkovic, B. Kasalica, Z. Nedic, L. Zekovic, Characterization of the plasma electrolytic oxidation of aluminium in sodium tungstate, Corrosion Science 52 (10) (2010) 3258–3265.
[29] W.B. Xue, Q.Z. Zhu, Q. Jin, M. Hua, Characterization of ceramic coatings fabricated on zirconium alloy by plasma electrolytic oxidation in silicate electrolyte, Materials Chemistry and Physics 120 (2–3) (2010) 656–660.
[30] A. Polat, M. Makaraci, M. Usta, Influence of sodium silicate concentration on structural and tribological properties of microarc oxidation coatings on 2017A aluminum alloy substrate, Journal of Alloys and Compounds 504 (2) (2010) 519–526.
[31] A.L. Yerokhin, X. Nie, A. Leyland, A. Matthews, Characterisation of oxide films produced by plasma electrolytic oxidation of a Ti–6Al–4V alloy, Surface & Coatings Technology 130 (2–3) (2000) 195–206.
[32] K.H. Nan, T. Wu, J.H. Chen, S. Jiang, Y. Huang, G.X. Pei, Strontium doped hydroxyapatite film formed by micro-arc oxidation, Materials Science & Engineering C-Biomimetic and Supramolecular Systems 29 (5) (2009) 1554–1558.
[33] W.H. Song, Y.K. Jun, Y. Han, S.H. Hong, Biomimetic apatite coatings on micro-arc oxidized titania, Biomaterials 25 (17) (2004) 3341–3349.
[34] S. Durdu, O.F. Deniz, I. Kutbay, M. Usta, Characterization and formation of hydroxyapatite on Ti6Al4V coated by plasma electrolytic oxidation, Journal of Alloys and Compounds 551 (2013) 422–429.
[35] M.S. Kim, J.J. Ryu, Y.M. Sung, One-step approach for nano-crystalline hydroxyapatite coating on titanium via micro-arc oxidation, Electrochemistry Communications 9 (8) (2007) 1886–1891.
[36] T. Hanawa, Biofunctionalization of titanium for dental implant, Japanese Dental Science Review 46 (2) (2010) 93–101.
[37] F. Liu, Y. Song, F.P. Wang, T. Shimizu, K. Igarashi, L.C. Zhao, Formation characterization of hydroxyapatite on titanium by microarc oxidation and hydrothermal treatment, Journal of Bioscience and Bioengineering 100 (1) (2005) 100–104.
[38] L.H. Li, H.W. Kim, S.H. Lee, Y.M. Kong, H.E. Kim, Biocompatibility of titanium implants modified by microarc oxidation and hydroxyapatite coating, Journal of Biomedical Materials Research Part A 73A (1) (2005) 48–54.
[39] M. Aliofkhazraei, A.S. Rouhaghdam, Wear and coating removal mechanism of alumina/titania nanocomposite layer fabricated by plasma electrolysis, Surface & Coatings Technology 205 (2011) S57–S62.
[40] X.J. Li, G.A. Cheng, W.B. Xue, R.T. Zheng, Y.J. Cheng, Wear and corrosion resistant coatings formed by microarc oxidation on TiAl alloy, Materials Chemistry and Physics 107 (1) (2008) 148–152.
[41] Y. Vangolu, A. Alsaran, O.S. Yildirim, Wear properties of micro arc oxidized and hydrothermally treated Ti6Al4V alloy in simulated body fluid, Wear 271 (9–10) (2011) 2322–2327.
[42] E. Arslan, Y. Totik, E.E. Demirci, I. Efeoglu, Wear and adhesion resistance of duplex coatings deposited on Ti6Al4V alloy using MAO and CFUBMS, Surface & Coatings Technology 214 (2013) 1–7.
[43] L.H. Li, Y.M. Kong, H.W. Kim, Y.W. Kim, H.E. Kim, S.J. Heo, J. Y. Koak, Improved biological performance of Ti implants due to surface modification by micro-arc oxidation, Biomaterials 25 (14) (2004) 2867–2875.
[44] F.C. Gennari, D.M. Pasquevich, Kinetics of the anatase rutile transformation in TiO_2 in the presence of Fe_2O_3, Journal of Materials Science 33 (6) (1998) 1571–1578.
[45] S. Durdu, A. Aytac, M. Usta, Characterization and corrosion behavior of ceramic coating on magnesium by micro-arc oxidation, Journal of Alloys and Compounds 509 (34) (2011) 8601–8606.
[46] A.L. Yerokhin, X. Nie, A. Leyland, A. Matthews, S.J. Dowey, Plasma electrolysis for surface engineering, Surface & Coatings Technology 122 (2–3) (1999) 73–93.
[47] Y. Han, S.H. Hong, K.W. Xu, Porous nanocrystalline titania films by plasma electrolytic oxidation, Surface & Coatings Technology 154 (2–3) (2002) 314–318.
[48] S. Durdu, M. Usta, Characterization and mechanical properties of coatings on magnesium by micro arc oxidation, Applied Surface Science 261 (2012) 774–782.
[49] E. Cakmak, K.C. Tekin, U. Malayoglu, S. Shrestha, The effect of substrate composition on the electrochemical and mechanical properties of PEO coatings on Mg alloys, Surface & Coatings Technology 204 (8) (2010) 1305–1313.
[50] A.V. Stanishevsky, S. Holliday, Mechanical properties of sol–gel calcium titanate bioceramic coatings on titanium, Surface and Coatings Technology 202 (4–7) (2007) 1236–1241.
[51] V. Gupta, K.K. Bamzai, P.N. Kotru, B.M. Wanklyn, Mechanical characteristics of flux-grown calcium titanate and nickel titanate crystals, Materials Chemistry and Physics 89 (1) (2005) 64–71.
[52] R.G. Bayer, Mechanical Wear Fundamentals and Testing, Revised and Expanded, Second ed., CRC Press, New York, USA, 2004.